JOURNAL OF AGRICULTURAL AND FOOD CHEMISTRY

Near-Infrared Imaging Spectroscopy Based on Sugar Absorption Band for Melons

MIZUKI TSUTA,*,†,‡ JUNICHI SUGIYAMA,† AND YASUYUKI SAGARA‡

National Food Research Institute, 2-1-12 Kan-nondai, Tsukuba, Ibaraki 305-8642, Japan, and
The University of Tokyo, 1-1-1 Yayoi, Bunkyo, Tokyo 113-8657, Japan

A method for visualizing the sugar content in the flesh of melons was developed. This method was based on the sugar absorption band in the near-infrared (NIR) region to avoid bias caused by the color information of a sample. NIR spectroscopic analysis revealed that each of the two second-derivative absorbances at 874 and 902 nm had a high correlation with the sugar content of melons. A high-resolution cooled charged couple device camera with band-pass filters, which included the above two wavelengths, was used to capture the spectral absorption image of a half-cut melon. A color distribution map of the sugar content on the surface of the melon was constructed by applying the NIR spectroscopy theory to each pixel of the acquired images.

KEYWORDS: Near-infrared; imaging; spectroscopy; sugar content; melon

INTRODUCTION

In Japan, the near-infrared (NIR) spectroscopy technique has been widely adopted in automated sweetness sorting machines for various fruits such as peaches, apples, and melons in 172 packing houses (*1*). Conventionally, a sorting machine measures the absorbance of the whole or a part of a fruit by a point-type detector and calculates the average sugar content by applying a calibration equation to the acquired absorbance data. Taste judgment by sorting machines may sometimes differ from taste judgment by consumers because of uneven distribution of sugar in a fruit. There have been some attempts to measure the distribution of sugar content by chemical analysis (*2*). However, the space resolution is low, and it takes a long time and much labor to extract and analyze many portions. Visualization of the sugar content of fruits is expected to be useful not only for evaluation of their taste quality but also for physiological analysis of their properties. Visualization methods using the NIR technique for measuring the distribution of sugar in a green-flesh melon and a kiwifruit have already been reported (*3*, *4*). The former method, however, cannot be applied to a red-flesh melon because it depends not on the absorption band of the sugar but on the color information at 676 nm. The objective of this research is to develop a universal method for visualizing the sugar content based on the absorption band of the sugar in the NIR wavelength region.

MATERIALS

Sample. Two green-flesh melons (Delicy) and three red-flesh melons (Quincy) were prepared for NIR spectroscopy, and another red-flesh melon (Quincy) was prepared for imaging. They were obtained from a store and left overnight in a dark room at 25 °C before the experiment. The experiments were carried out in the same room.

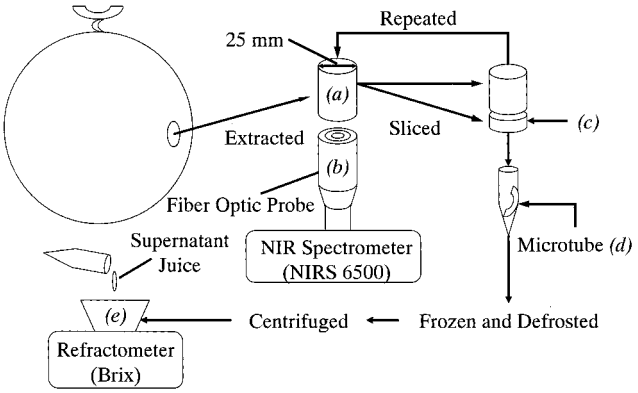

Figure 1. NIR spectroscopy of melons.

Instrumentation for NIR Spectroscopy. To specify the absorption band of sugar, an NIR spectrometer (NIRS 6500, FOSS NIRSystems, Silver Spring, MD) and a digital refractometer (PR-100, ATAGO, Yorii, Saitama, Japan) were utilized (Figure 1). Pretreatment of the acquired spectra and a multilinear regression (MLR) analysis were carried out using spectral analysis software (VISION, FOSS NIRSystems).

Imaging System. Figure 2 shows the configuration of the apparatus for obtaining spectroscopic images. The cooled charged couple device (CCD) camera (CV-04 II, Mutoh Industries Ltd., Tokyo, Japan) had a 16-bit (65536 steps) A/D resolution, a linear intensity characteristic ($\gamma = 1$), and no antiblooming gate, so that each pixel could function as a detector of an NIR spectrometer for quantitative analysis. To decrease the electrical dark current noise of the CCD camera, both double-stage thermoelectric cooling and water cooling were utilized. A filter adapter with a filter holder (Koueisha, Kawagoe, Saitama, Japan) and a camera lens (FD28 mm F3.5 S. C., Canon, Tokyo, Japan) were installed in the CCD camera. The filter holder had four holes to which four filters could be fitted. The four filters in this experiment

* Authors to whom correspondence should be addressed (fax +81-298-39-1552; e-mail mizukit@affrc.go.jp or sugiyama@affrc.go.jp).
† National Food Research Institute.
‡ The University of Tokyo.

10.1021/jf010854i CCC: $22.00
Published on Web 12/06/2001

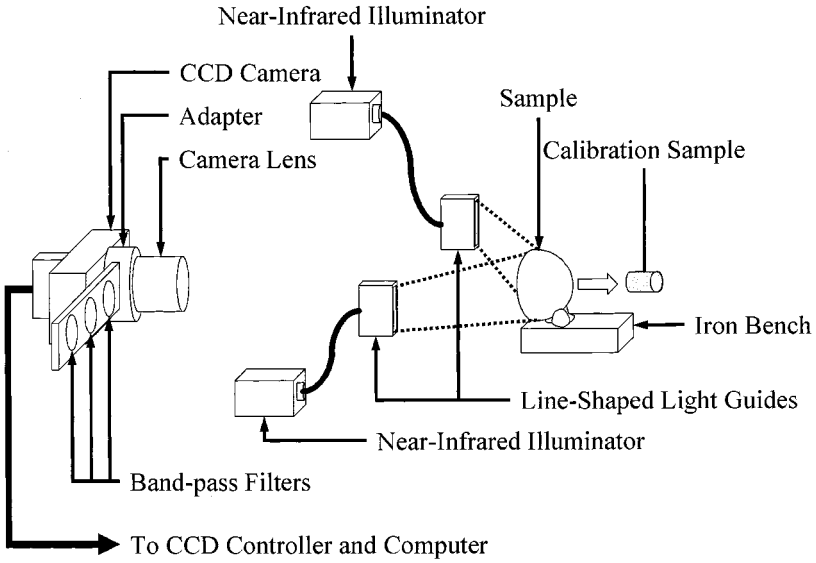

Figure 2. Imaging system.

(BWE*x*; x = 846, 874, 902, 930, Koshin Kogaku Filters, Hatano, Kanagawa, Japan) were designed to have band-pass characteristics of *x* nm at the central wavelength, and their details are shown in Table 1. The wavelengths of 902 and 874 nm were determined in the NIR spectroscopic experiment (see Methods and Results and Discussion), and the others were their neighboring wavelengths selected to calculate the second-derivative absorbances. The near-infrared illuminator (LA-100IR, Hayashi Watch-Works, Tokyo, Japan) irradiated only near-infrared light because a near-infrared reflecting mirror was installed around a tungsten−halogen bulb, and a high-pass filter, which transmits only light above 800 nm, was attached to the irradiation hole. The source light was introduced into line-shaped light guides through a fiber optic probe, illuminating a sample from two different positions so as not to create any shadows or direct reflection. Previously, we placed a quartz glass on the surface of the sample to maintain a constant focal distance between the CCD camera and the sample (*3*). In this experiment, however, a direct reflection image of the CCD camera on the glass was observed because the intensities of the sample and unnecessary images were both low; these were enhanced by a long exposure period. Therefore, the quartz glass was not adopted in this experiment; instead, the sample was placed on an iron bench facing the camera.

METHODS

Calculation of Second-Derivative Spectrum. Derivative methods are important pretreatment methods in NIR spectroscopy. The second-derivative method is most often used because of its following merits (*5*, *6*):

1. Positive peaks in a raw spectrum are converted into negative peaks in a second-derivative spectrum.
2. The resolution is enhanced for the separation of overlapping peaks and the emphasis of small peaks.
3. The additive and multiplicative baseline shifts in a raw spectrum are removed.

By applying the truncated Taylor series expansion, a second-derivative spectrum can be calculated as follows (*7*):

$$f^2(x) = \frac{f(x + \Delta x) - 2f(x) + f(x - \Delta x)}{\Delta x^2} \quad (1)$$

Here, $f(x)$ is the spectral function at x and $f^2(x)$ is the second-derivative function at x. Actual spectral data, however, take discrete values because of the limited wavelength resolution of NIR spectrometers. Therefore, a second-derivative spectrum is calculated as follows in NIR spectroscopy (*5*):

$$d^2A_i = A_{i+k} - 2A_i + A_{i-k} \quad (2)$$

Table 1. Characteristics of the Band-Pass Filters

model	central wavelength (nm)		bandwidth (nm)
	specified value	measured value	
BWE846 ϕ 30	846.0 ± 2.0	847.5	13.3
BWE874 ϕ 30	874.0 ± 2.0	875.8	13.6
BWE902 ϕ 30	902.0 ± 2.0	900.0	16.0
BWE930 ϕ 30	930.0 ± 2.0	928.5	16.0

Here, A_i is the absorbance at i nm, d^2A_i is the second-derivative absorbance at i nm, and k is the distance between the neighboring wavelengths, which is called a derivative gap. Equation 2 shows that absorbances at three wavelengths of i, $i + k$, and $i - k$ are sufficient for calculating the second-derivative absorbance at i nm. It also indicates that the imaging system can acquire a second-derivative spectroscopic image using three band-pass filters.

NIR Spectroscopy. A 25-mm-diameter cylindrical sample (Figure 1a) was extracted from the "equator" of a melon using a stainless steel cylinder with a knife-edge at one end. A spectrum of the sample's inner surface was obtained using a fiber optic probe (Figure 1b) of the NIR spectrometer in the interactance mode (*8*). The wavelength interval was 2 nm, and the number of scans was 50. The measured portion was then cut into a 1-mm-thick slice (Figure 1c) using a handicraft cutter and put into a 1.5-mL microtube (Figure 1d) to be frozen and defrosted. This process was intended to break the cell walls of the portion in order to extract a sufficient amount of juice for measuring the sugar content (*4*). The portion was then centrifuged for 10 min at 10000 rpm to extract juice. The °Brix sugar content of the juice was measured using the digital refractometer (Figure 1e). A set of the spectrum and the sugar content measurements for every 1-mm-thick slice was repeated from the inner surface toward the rind (Figure 1b → 1c → 1d → 1e → 1b . . .). Each raw spectrum was converted into a second-derivative spectrum to decrease the effect of spectral baseline shifts (*5*, *6*). An MLR analysis was carried out for all of the data sets to acquire the calibration curve for the sugar content and the second-derivative spectra.

Acquisition of the Spectroscopic Images. Using the imaging system, whole images of the surface of a half-cut sample were taken at 846, 874, 902, and 930 nm at an exposure period of 3.7 s. The binning mode of 2 × 2, that is, four pixels of the CCD camera were combined to function as one pixel, was applied to acquire a higher sensitivity (*9*). The temperature of the CCD camera was maintained at −20 °C. The size of the image was 384 × 256 pixels after binning. After a half-cut image had been captured, two 25-mm-diameter cylindrical samples were extracted from the "equator" of the same melon. These cylindrical samples were used to acquire a sugar content calibration curve based on the imaging system. In the same manner as in the case of a half- cut sample, images of the surface of the cylindrical samples

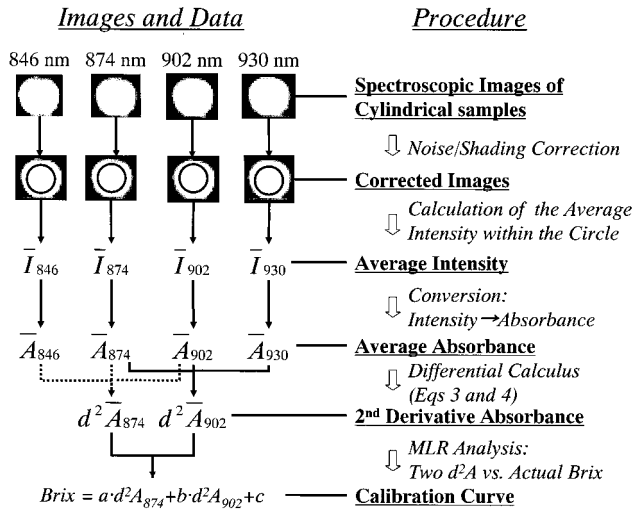

Figure 3. Image processing procedure for calibration.

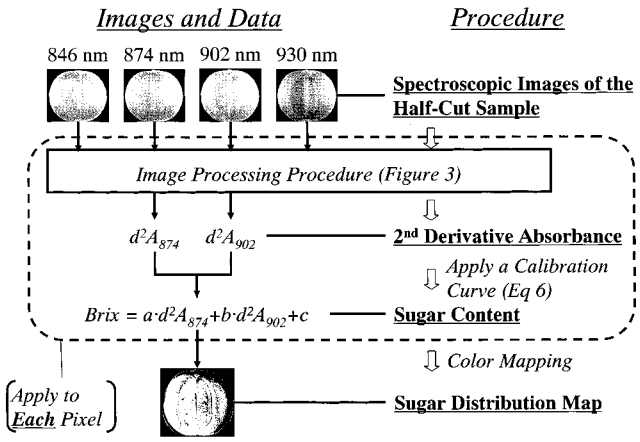

Figure 4. Visualization procedure.

were taken, after which a 1-mm-thick slice was obtained and the °Brix sugar content was measured as described for the NIR spectroscopic experiment (Figure 1). Image capture and measurement of the sugar content were repeated until the rind appeared.

Image Processing for Calibration. The obtained raw images of the cylindrical samples include (1) thermal noise, (2) bias signals to offset the CCD slightly above zero A/D counts, (3) sensitivity variations from pixel to pixel on the CCD, and (4) lighting variations on the samples surface (*9*). To compensate for the above effects, noise and shading corrections were carried out for all images. The average intensity of the images of the cylindrical sample was converted into the average absorbance based on the spectroscopy theory (Figure 3). These processes were described in a previous paper (*3*). Once the average absorbance at each wavelength was obtained, the second-derivative absorbances at 902 and 874 nm were calculated as follows (*5*, *7*) (see Methods):

$$d^2A_{902} = A_{930} - 2A_{902} - A_{874} \quad (3)$$

$$d^2A_{874} = A_{902} - 2A_{874} - A_{846} \quad (4)$$

Here, A_i is the absorbance at i nm and d^2A_i is the second-derivative absorbance at i nm. Then, MLR analysis using these second-derivative absorbances was carried out to acquire the calibration curve for the sugar content on the imaging system.

Sugar Mapping. The intensity of each pixel on the half-cut sample image was converted into the second-derivative absorbances at 902 and 874 nm in the same manner as in the case of cylindrical samples (Figure 4). The acquired calibration curve was applied to these two second-derivative absorbances at each pixel in order to calculate the sugar content. Finally, the sugar content was visualized by mapping the value with a linear color scale. Image processing software, which we developed, was utilized to process images and to construct a sugar distribution map.

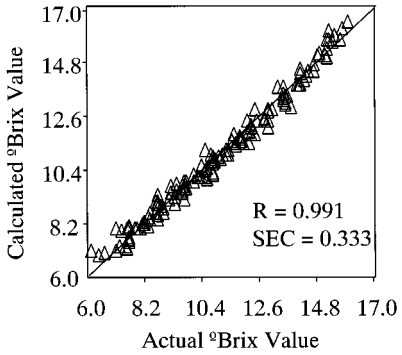

Figure 5. Calibration by NIR spectroscopy.

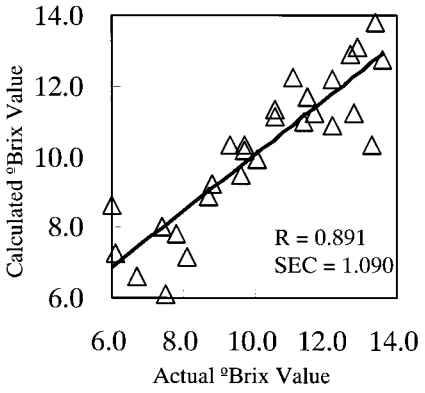

Figure 6. Calibration by imaging.

RESULTS AND DISCUSSION

Absorption Band of Sugar by NIR Spectroscopy. One hundred and fifty-seven spectra were obtained as a result of NIR spectroscopy, and the MLR analysis of the spectra revealed that the second-derivative absorbances at 874 and 902 nm were highly correlated with the sugar content as shown in Table 2. The correlation was maintained at a high level, ~0.99, whereas the derivative gap changed from 20 to 36 nm. The derivative gap was selected to decrease the number of band-pass filters for the imaging system. Conventionally, six band-pass filters are necessary to acquire two second-derivative spectroscopic images. When the derivative gap of 28 nm was adopted, however, only four band-pass filters, that is, 846, 874, 902, and 930 nm, were sufficient for the analysis. This is because 874 and 902 nm overlapped between two second derivatives (indicated in bold letters in Table 2). When 28 nm was selected as the derivative gap, the calibration curve was as follows:

$$°\text{Brix} = 21.93 - 410.76\, d^2A_{902} + 1534.76\, d^2A_{874} \quad (5)$$

The curve had a high correlation with the sugar content (R = 0.991), and the standard error of calibration was 0.333 (Figure 5). The second-derivative absorbance at 902 nm had an inverse correlation with the sugar content, which indicated that the raw absorbance had a positive correlation with it. In addition, several publications (*8*, *10*−*13*) indicated that 902 nm is one of the typical absorption bands of sugar components. On the other hand, 874 nm can be considered as the reference wavelength to compensate for different surface conditions or some other influences. As a result, four band-pass filters of 846, 874, 902, and 930 nm were adopted for the imaging system.

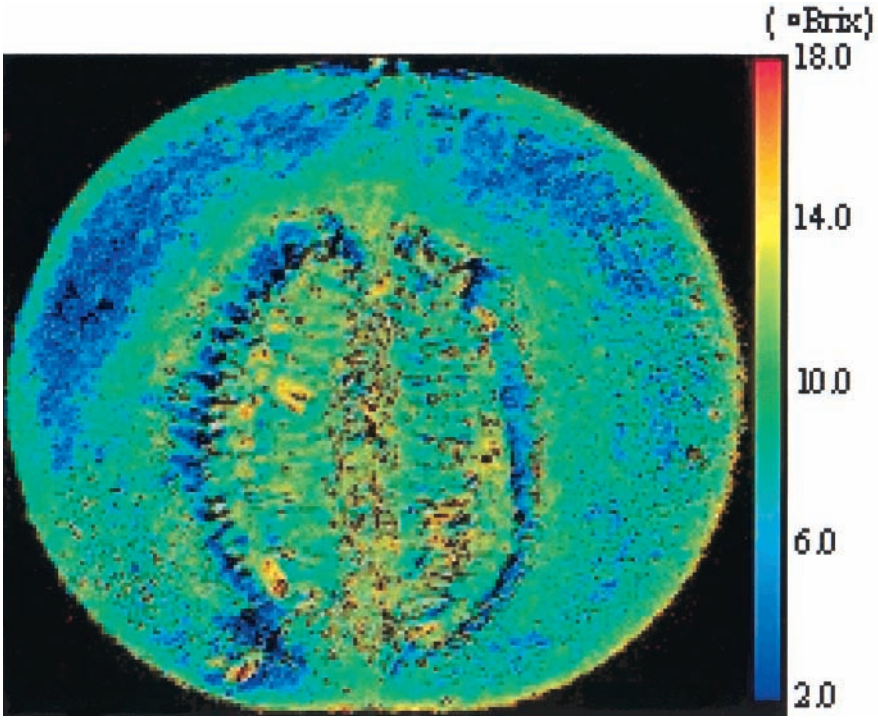

Figure 7. Sugar distribution map.

Table 2. Relationship among the Derivative Gap, Correlation, and Necessary Band-Pass Filters

		necessary band-pass filters (nm)					
gap (nm)	*R*	for d^2A_{874}			for d^2A_{902}		
4	0.976	870	874	878	898	902	906
8	0.975	866	874	882	894	902	910
12	0.983	862	874	886	890	902	914
16	0.988	858	874	890	886	902	918
20	0.990	854	874	894	882	902	922
24	0.991	850	874	898	878	902	926
28	0.991	846	***874***	***902***	***874***	***902***	930
32	0.991	842	874	906	870	902	934
36	0.990	838	874	910	866	902	938
40	0.988	834	874	914	862	902	942

Calibration by the Imaging System. A calibration curve for the second-derivative absorbance and the sugar content in the imaging system was obtained by MLR analysis of 33 slices from the cylindrical samples (Figure 6).

$$°\text{Brix} = 19.01 - 438.84\ \text{d}^2A_{902} + 70.32\ \text{d}^2A_{874} \qquad (6)$$

The second-derivative absorbance at 902 nm had an inverse correlation with the sugar content in eq 6, which is the same as in eq 5. It had a high correlation of $R = 0.891$, and the standard error was 1.090. It can be considered that the imaging system adopted in this study has sufficient capability to visualize the sugar content.

Visualization of Sugar Distribution. A sugar distribution map of the half-cut red-flesh melon was constructed by applying eq 6 to each pixel of the processed images (Figure 4). In Figure 7, sugar contents ranging from 2 to 18 °Brix were assigned with a linear color scale. The color changes gradually from blue to red as the sugar content increases. Although it was difficult to differentiate the sugar distribution by the naked eye, Figure 7 shows that the sugar content increases from the rind to near the seeds. It also indicates that the central upper part of the sample was sweeter than the bottom part, which is the reverse of the general notion in Japan. These results suggest that NIR imaging could become a useful method for evaluating the distribution of sugar in melons. In addition, further studies may lead to the application of this method to not only various varieties of melons but also other constituents of other agricultural products because it does not depend on color information.

ACKNOWLEDGMENT

We gratefully thank Dr. Sumio Kawano for worthful advice on NIR spectroscopy.

LITERATURE CITED

(1) Hasegawa, Y. Merits and Demerits of the Automated Sweetness Sorting Techniques. *Fresh Food Syst*. **2000**, *30*, 74−77.
(2) Ishigami, K.; Matsuura, H. Studies on the Sugar Distribution and Composition of Muskmelon Fruit. *Bull. Shizuoka Agric. Exp. Stn.* **1993**, *37*, 33−40.
(3) Sugiyama, J. Visualization of Sugar Content in the Flesh of a Melon by Near-Infrared Imaging. *J. Agric. Food Chem*. **1999**, *47*, 2715−2718.
(4) Martinsen, P.; Schaare, P. Measuring Soluble Solid Distribution in Kiwifruit Using Near-Infrared Imaging Spectroscopy. *Postharvest Biol. Technol.* **1998**, *14*, 271−281.
(5) Katsumoto, Y.; Jiang, J.; Berry, R. J.; Ozaki, Y. Modern Pretreatment Methods in NIR Spectroscopy. *Near Infrared Anal.* **2001**, *2*, 29−36.
(6) Iwamoto, M.; Kawano, S.; Uozumi, J. Data Processing Method. In *Kin-Sekigai Bunkouhou Nyuumon*; Saiwai Shobou: Tokyo, Japan, 1994; pp 62−95.
(7) Morimoto, S.; McClure, W. F.; Stanfield, D. L. Hand-Held NIR Spectrometry: Part I: An Instrument Based upon Gap-Second Derivative Theory. *Appl. Spectrosc.* **2001**, *55*, 182−189.
(8) Kawano, S.; Watanabe, H.; Iwamoto, M. Determination of Sugar Content in Intact Peaches by Near Infrared Spectroscopy with Fiber Optics in Interactance Mode. *J. Jpn. Soc. Hortic*. **1992**, *61*, 445−451.
(9) Fukushima, H. How to Use the CCD Camera. In *Reikyaku CCD nyuumon*; Sibundou Sinkousha: Tokyo, Japan, 1996; pp 73−132.

(10) Kawano, S.; Fujiwara, T.; Iwamoto, M. Nondestructive Determination of Sugar Content in Satsuma Mandarin Using Near Infrared (NIR) Transmittance. *J. Jpn. Soc. Hortic. Sci*. **1993**, *62*, 465−470.

(11) Kawano, S.; Abe, H. Development of a Calibration Equation with Temperature Compensation for Determining the Brix Value in Intact Peaches. *J. Near Infrared Spectrosc*. **1995**, *3*, 211−218.

(12) Ito, M.; Iida, J.; Terashima, A.; Kishimoto, T. Non-Destructive Sugar Content Measuring Method (Japanese Patent). JP 08-327536 A, 1996.

(13) Temma, M.; Hanamatsu, K.; Shinoki, F. Development of a Compact Near-Infrared Apple-Sugar-Measuring Instrument and Applications. In *Proceedings of the 15th Symposium on Non-Destructive Measurements*; Tsuyuki, H., Ed.; Japanese Society for Food Science and Technology: Ibaraki, Japan, 1999; pp 113−117.

Received for review July 3, 2001. Revised manuscript received October 9, 2001. Accepted October 11, 2001.

JF010854I